Journal of Atmospheric and Solar–Terrestrial Physics 211 (2020) 105461

Contents lists available at ScienceDirect

Journal of Atmospheric and Solar-Terrestrial Physics

journal homepage: www.elsevier.com/locate/jastp

GPS derived amplitude scintillation proxy model: A case over a low latitude station in East Africa

Geoffrey Andima [a,*], Emirant B. Amabayo [a,b], Edward Jurua [a], Pierre J. Cilliers [a,c]

[a] Department of Physics, Mbarara University of Science and Technology, Mbarara, Uganda
[b] Department of Physics, Busitema University, Tororo, Uganda
[c] South African National Space Agency (SANSA) Space Science, Hermanus, South Africa

ARTICLE INFO

Keywords:
Ionospheric scintillation
Low latitude irregularities
Scintillation proxy
Scintillation model

ABSTRACT

Ionospheric scintillation is quite a common phenomenon over the low latitude regions and in East Africa it is often monitored using measurements from the SCIntillation Network Decision Aid (SCINDA) receivers. The SCINDA receivers over East Africa are characterized by long base lines and data paucity thus offering a huge challenge in the long term scintillation characterization over the region. To alleviate this challenge, we implemented the use of data from the dual frequency GPS receivers of the IGS network in combination with data from the SCINDA receiver at Nairobi, Kenya to model amplitude scintillation. The data from the SCINDA (geographic coordinates 36.808°E, −1.274°N) and GPS (geographic coordinates 36.893°E, −1.221°N) receivers were used to derive S4 index and its proxy respectively. Comparison of the S4 and its proxy revealed a high correlation coefficient between the two datasets. Scintillation occurrence was observed to peak during the equinox months of March–April and September–October. The vernal equinox was observed to have less frequent scintillation events than the autumnal equinox. The local time (LT) scintillation occurrence shows a peak between 20:00 LT and 23:00 LT. An empirical hybrid amplitude scintillation occurrence probability model was then developed. The results show that the model predicted values were in good agreement with the observed amplitude scintillation occurrence probabilities from the SCINDA receiver. This observation suggests that the model is a useful tool for approximating amplitude scintillation occurrence probabilities at L-band frequencies at African equatorial latitudes.

1. Introduction

Of great concern to ionospheric scientists and communication engineers is the need to provide accurate and reliable situational information on when and where one can rely on satellite communication. This concern is due to the fact that satellite radio signals are refracted or diffracted or both when they enter a layer of irregularities in the ionosphere. The scattered signals add at the receiver unit to produce amplitude and or phase scintillation resulting in signal fades. Deep signal fades may cause the receiver to loose track of the signal. If a significant number of satellite links are lost simultaneously, the system cannot provide required information until lock is reacquired on a sufficient number of links, thus hampering communication. Ionospheric scintillation over the low latitudes have been observed to be frequent. Instabilities of Rayleigh Taylor type are believed to be the main cause of equatorial irregularities (Kelley, 2009). Therefore scintillation measurements have been used to infer the characteristics of the irregularities and hence the changing patterns of their driving forces. In the rest of this paper, only amplitude scintillation has been considered and for simplicity, the term scintillation has exclusively been used to refer to amplitude scintillation.Scintillation is usually quantified by the S4 index defined as the standard deviation of the received signal intensity normalized by its mean value. The S4 index is often obtained from some specialized scintillation monitors. Few such receivers exist over the low latitudes, let alone the difficulty of having their data available for public use. In addition to the long base lines, data paucity from these receivers has made complete characterization of low latitude ionospheric scintillation quite difficult. The relationship between time series total electron content (TEC) variations and scintillation causing irregularities has been explored to overcome the limited geographical coverage by the standard scintillation monitors (Aarons et al., 1996, 1997). These studies focused on the TEC fluctuations as a measure of the presence of

* Corresponding author.
E-mail address: geoffrey.andima@gmail.com (G. Andima).

https://doi.org/10.1016/j.jastp.2020.105461
Received 30 May 2020; Received in revised form 16 September 2020; Accepted 17 September 2020
Available online 5 October 2020
1364-6826/© 2020 Elsevier Ltd. All rights reserved.

the scintillation causing irregularities. A common observation is that the amplitude of a radio signal is sensitive to the TEC fluctuations. Pi et al. (1997) introduced an index based on the TEC fluctuations, called rate of change of TEC index (ROTI), which is the standard deviation of rate of change of TEC (ROT) to characterize ionospheric irregularities. Many authors have validated the ROTI index against S4 measurements from standard scintillation monitors (e.g. Basu et al., 1999; Beach and Kintner (2009); Zou and Wang 2009). In some cases, ROTI has been used to develop models to forecast the occurrence of irregularities (e.g Mungufeni et al., 2015). Though a good correlation has been observed between S4 and ROTI in many of these studies, a renewed challenge that emerged is to find an appropriate scaling factor to scale either S4 or ROTI to match the other. To try to address this challenge, Beach and Kintner (2009) derived a multiplicative factor to convert ROTI to S4 and this factor varied from one night to another between 0.2 and 0.5. A theoretical relationship was envisaged between S4 and ROTI, and this relationship was dependent on the projection of the satellite velocity, irregularity velocity, and the slant distance of the irregularities from the receiver (Bhattacharya et al., 2009). Based on this, Bhattacharya et al. (2009) proposed a new index, DROTI, which is the standard deviation of the derivative of ROT. They observed that DROTI or ROTI could separately be scaled to match S4 index using scaling factors of 5 and 2.5 respectively. Since then, occasionally both scaled ROTI and scaled DROTI have been used to characterize ionospheric irregularities (e.g. Du et al., 2000; Amabayo et al., 2015). The scaling factors used by the different authors have largely not been consistent. For instance Du et al. (2000) in a study at the southern crest of the equatorial ionisation anomaly used a factor of 2.5 to scale ROTI to match the S4 values. In a similar study over a low latitude region, Amabayo et al. (2015) obtained a scaling factor of ~10 between ROTI and S4. The reason for these variations is largely unknown. However, one factor that has been ignored in these two studies is the variation of the projected satellite velocity at the ionospheric pierce point (IPP) and the time variation of the drift velocity of irregularities. The projected satellite velocity at the IPP is dependent on the elevation angle of the satellite, while earlier studies (e.g. Rao et al., 2005; Andima et al., 2018) reported temporal variations in the drift velocity of equatorial irregularities. Both Du et al. (2000) and Amabayo et al. (2015) considered the projected satellite velocity and the drift velocity of irregularities as constants, and this may potentially contribute to the different scaling factors they obtained. The objective of this paper is to derive a scintillation proxy from TEC fluctuations obtained from the dual frequency IGS receivers using time varying ion drift velocity. The proxy is then validated using scintillation data from co-located scintillation monitors. The S4 proxy is to be combined with the S4 index to model scintillation occurrence. The combination of S4 index with the S4 proxy is expected to provide opportunity for a better detection and characterization of ionospheric scintillation for possible space weather forecast.

2. Data and methods

A sizable number of ground based instruments have been deployed over the African low latitude region for ionospheric monitoring. Of these are the SCINDA receivers of the Air Force Research Laboratory (AFRL), and the dual frequency GPS receivers of the International GNSS Service (IGS) network. In this study, data from SCINDA receivers at Nairobi nearly co-located with the IGS receiver were used.

Table 1 gives the coordinates of the ground receivers that were used in this study. The TEC from which the ROT was derived were extracted from the IGS RINEX files using the GPS-TEC software of Boston college (Seemala and Valladares, 2011). The ROT was calculated according to the equation

$$\mathrm{ROT} = \frac{\mathrm{TEC}^k_{i+1} - \mathrm{TEC}^k_i}{t_{i+1} - t_i}, \tag{1}$$

Table 1
The locations of the ground GPS in fracture from which data used in this study was obtained.

Station			Geographic		Geomagnetic	
Place	Type	Code	Lon (°E)	Lat (°N)	Lon (°E)	Lat (°N)
Mbarara	IGS	MBAR	30.738	−0.601	102.730	−11.415
Mbarara	SCINDA	MBA	30.656	−0.616	102.647	−11.448
Nairobi	IGS	RCMN	36.893	−1.221	108.964	−10.836
Nairobi	SCINDA	UON	36.808	−1.274	108.878	−10.906
Nairobi	VHF	VHF	36.808	−1.274	108.878	−10.906

where k is the index of the visible satellite and i is the time of epoch. The ROT value for each satellite was then detrended for elevation angles greater than 50°. The standard deviation of the detrended ROT was then calculated over 5 min running window to obtain ROTI. Two different methods were applied to the same data set to scale ROTI to match S4 as closely as possible. One method makes use of the transport of intensity equation (Teague, 1983) to derive an approximate relation between the phase and intensity variations after the ray has passed through the phase screen. The other method uses the weak scatter theory (Rino, 1979) to relate ROTI and S4 (Carrano et al., 2019). We have referred to these methods as method1 and method2 respectively in our subsequent discussions.

2.1. method1

Bhattacharya et al. (2009) using transport of intensity equation (Teague, 1983) derived an approximate relation between the signal intensity $I_{(x,z)}$ measured by a ground receiver and the transverse phase variations ϕ_x imposed by a layer of irregularities as

$$\frac{d^2\phi_x}{dx^2} = -\frac{2\pi}{\lambda r_e}\left[1 - \frac{I_{(x,z)}}{I_o}\right], \tag{2}$$

where r_e is the classical electron radius (2.8×10^{-15} m), I_o is the signal intensity before entering the layer of irregularities and λ is the wavelength of the radio signal. The spatial variations in equation (2) are converted to temporal variations, often recorded by typical scintillation receivers, using the transverse plasma velocity relative to the IPP velocity. Bhattacharya et al. (2009) expressed such a temporal variation in terms of the electron density variations as

$$\frac{d^2\Delta N_e}{dt^2} = -\frac{2\pi}{\lambda^2 r_e}\frac{V^2}{z}\left[1 - \frac{I_{(t,z)}}{I_o}\right], \tag{3}$$

where V is the average drift speed of the irregularities transverse to the signal path and z is the distance of the receiver along the ray path to the irregularity layer. The standard deviation of $d^2\Delta N_e/dt^2$ and $\left[1 - \frac{I_{(t,z)}}{I_o}\right]$ give the DROTI (Bhattacharya et al., 2009) and the S4 indexes respectively. Though it would be natural to use DROTI to estimate S4, Du et al. (2000) observed that S4 can be extracted from both ROTI and DROTI in a similar way with the same accuracy. Since ROTI has been widely used to characterize irregularities, in this paper we have used ROTI instead of DROTI. Therefore, the scintillation proxy (S4p) was then calculated from equation (3) by scaling the ROTI as (Bhattacharya et al., 2009; Du et al., 2000)

$$\mathrm{S4P} = \gamma\mathrm{ROTI}, \tag{4}$$

where γ is the scaling factor given by $\gamma^{-1} = 2\pi V^2/\lambda^2 r_e z$. Bhattacharya et al. (2009) estimated the unknown velocity in the scaling factor from the Fresnel frequency which is often estimated from high rate data, while Du et al. (2000) used the satellite velocity relative to the earth and the plasma velocity to estimate V. The challenge with the latter approach is that the IPP velocity is invariant on the earth's surface which

is not realistically correct. The IPP velocity is dependent on the zenith angle. In this work, the velocity V was calculated from

$$V = V_d - \left(V_{py} - \tan\theta \sin\phi V_{pz}\right), \tag{5}$$

where V_d is the zonal component of the plasma velocity, V_{py} and V_{pz} are the ray path velocities in magnetic eastward and downward directions respectively. The velocities V_{py} and V_{pz} were determined from the precise orbit files available at ftp://ftp.nga.mil/pub2/gps/apcpe/ in a similar way as in Andima et al. (2018). The angles θ and ϕ are the nadir and the azimuth angles at the IPP respectively.

2.2. method2

In order to scale ROTI to S4, Carrano et al. (2019) showed that in the infinite axial ratio limit, typical of the equatorial irregularities, the ratio of ROTI to S4 can be expressed as

$$\frac{\mathrm{ROTI}^2}{\mathrm{S4}^2} = \frac{c^2}{\delta t^2}\left\{\frac{2^{1-2\nu}}{\Gamma(\nu)}\sqrt{\pi}\,\mathrm{cosec}\left[\frac{\pi}{4}(1+2\nu)\right]\right\}\left|\frac{V_{eff}}{\rho_F}\right|^{2\nu-1}, \tag{6}$$

where δt is the sampling rate, ν is the spectral index, $\rho_F^2 = z\lambda\sec\theta/\,2\pi$ is the square of the Fresnel filtering parameter and c is a parameter to convert phase measurement in radians to TEC units. The effective scan velocity V_{eff}, in equation (6) is defined in equation 13 of Rino (1979) as

$$V_{eff}^2 = \frac{CV_{px}^2 - BV_{px}V_{py} + AV_{py}^2}{AC - B/4}, \tag{7}$$

where V_{px} is the magnetic northward component of the ray path velocity at the IPP and the coefficients A, B and C were calculated following equations 28 of Carrano et al. (2016). We used equation (6) with $c =$ 0.186523 TECU/rad (Carrano et al., 2019) to obtain the scaling factor which was used to scale ROTI to S4. Well aware of the variation of ν, for simplicity we used a constant value of $\nu = 1.25$ which is supported by some observations (e.g. Carrano and Groves, 2010) of spectral index in the equatorial ionosphere. Following equation (6), S4p was expressed as

$$\mathrm{s4p} = \alpha\mathrm{ROTI}, \tag{8}$$

where α^{-2} is given by the right hand term of equation (6). The use of S4P and s4p in equation (4) and equation (8) is deliberate because the two values may not necessarily be the same. The scintillation proxy for weak scatter on which the theory described is based was obtained from equation (8) by applying the Rician statistics as

$$(\mathrm{S4Pw})^2 = 1 - \exp\{-(\mathrm{s4p})^2\} \tag{9}$$

2.3. The model

The S4p values for each satellite in view were averaged at every epoch and used to model the occurrence of scintillation. The time series data was first organized in solar flux bins of F10.7<80, 80≤F10.7<120 and F10.7≥120 to represent low, medium and high solar activity periods respectively. The data in each solar flux bin was further divided into monthly bins. Monthly average of the hourly occurrence probabilities of scintillation was computed by expressing the number of scintillation events as a fraction of the total number of observations in a given hour. The scintillation occurrence probability as a function of the local time (t), month (m) and solar activity (F10.7) was expressed as a simultaneous tensor product of the univariate cubic basis-splines (B-splines) as

$$\mathrm{F}(t, m, F10.7) = \sum_{i=1}^{13}\sum_{j=1}^{12}\sum_{k=1}^{3} c_{i,j,k}B_{i,4}(t)B_{j,2}(m)B_{k,2}(F10.7), \tag{10}$$

where $B_{i,4}(t)$ is a cubic B-spline of order four applied to local time. $B_{j,2}(m)$ and $B_{k,2}(F10.7)$ are cubic B-splines of order two applied to the month and the solar activity dependences respectively. The coefficients $c_{i,j,k}$ were determined by a least squares fit to the scintillation occurrence probabilities. The 13 knots for local time were placed at every hour from 18:00 LT to 2:00 LT. However, the knots between 19:00 LT and 23:00 LT were placed after every 30 min since scintillation activity maximizes around the same time. The monthly knots were placed on the 15th day of each month expressed in term of their DOY numbers. The solar flux nodes used in the model were determined in a similar way as in the work of other authors (e.g. Abdu et al., 2003; Iyer et al., 2006; Mungufeni et al., 2015).

3. Results and discussions

3.1. Scintillation and zonal drift velocity of irregularities

At equatorial latitudes, scintillation of satellite signals recorded on ground are typical of plasma density depletions which form bubbles in the F layer. The bubbles are believed to evolve nonlinearly, rise into the F layer, and then drift zonally across the satellite receiver links (Kelley, 2009). As they drift, diffraction of radio signals intercepted by these irregularities produce a scintillation pattern across the receiver. Fig. 1 shows VHF and L-band scintillation recorded over Nairobi on DOY 171 and DOY 267 in 2011.

The velocities shown in the top panels of Fig. 1 were computed for VHF S4 values that exceeded the noise level of 0.2. From Fig. 1 a, scintillation at VHF and L-band started at about 22:30 LT. The scintillation was due to plasma irregularities that drifted east-west at ~80 m/s. The velocity of the irregularities decreased to ~40 m/s at about 00:30 LT and then slightly increased to ~55 m/s between 02:00 and 03:00 LT. Though L-band scintillation ceased just after local midnight, VHF scintillation was seen to decrease gradually from 23:30 to 00:30 LT and then a slight increase at about 02:00 LT. A similar observation of simultaneous VHF and L-band scintillation is shown in Fig. 1 b. The scintillation started about 19:00 LT caused by irregularities that drifted with velocity in the range 120–150 m/s. The scintillation was observed to peak at about 21:00 to 23:00 LT, the same time when the maximum east-west irregularity velocities were observed. Though not an explicit relation, the intensity of the scintillation is in general depended on the drift velocity. This dependence has been exploited further in an attempt to scale ROTI to closely match the S4 values.

3.2. Scaled ROTI compared with S4

Scaling ROTI to get a close match with S4 has been reported in literature (Bhattacharya et al., 2009; Carrano et al., 2019). Generally, two approaches have been used in the papers cited above that is the transfer of intensity equation approach used by Bhattacharya et al. (2009) and the weak scatter theory approach used by Carrano et al. (2019). The two methods were then applied to the same data in an attempt to answer the question whether the differences in the scaling factors by the previous authors were due to the difference in the data or the methods used. Fig. 2 shows the variation of the line-of-sight TEC, S4 and ROTI indexes for four different days when there was simultaneous VHF and L-band scintillation.

Fig. 2 a shows that signals from PRN 22 encountered plasma density irregularities from about 23:30 to 01:00 LT as evidenced in the TEC. The TEC fluctuations were at high elevation angle and therefore were not due to multipath effect. The S4 index from the SCINDA on the same satellite link reached a moderate value of ~0.3 during the time when the TEC fluctuations were observed. The conventional ROTI calculated from co-located IGS TEC for PRN 22 showed a maximum value of ~1.5 TECU/min at the time when the irregularities were encountered by the satellite signal from PRN 22. The ROTI was well correlated with the S4 index. Our purpose is to scale the ROTI to numerically match S4 as much as possible. Both S4P and S4Pw are numerically more close to S4 than the conventional ROTI. In Fig. 2 b is a case when the signals from PRN 22

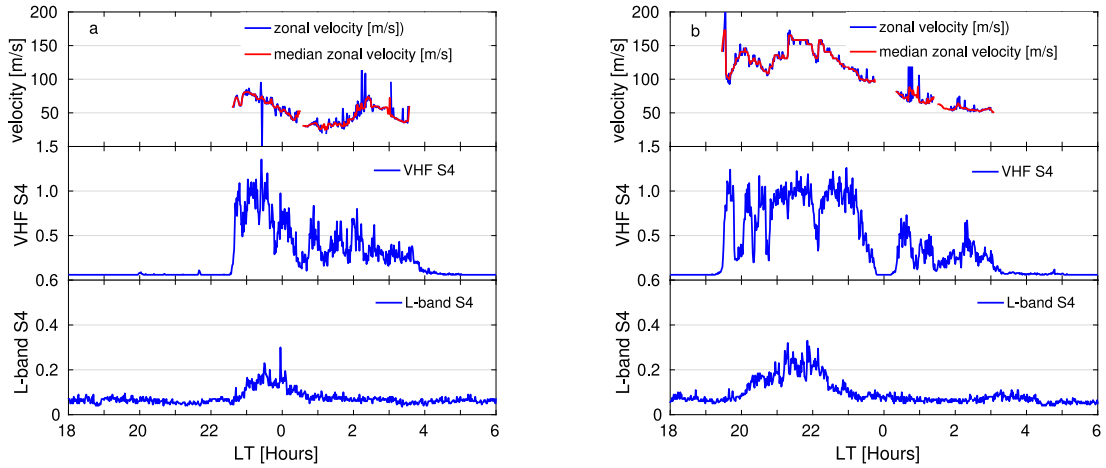


Fig. 1. Variation of VHF (middle panel) and L-band (bottom panel) scintillation, and zonal drift velocity of irregularities (top panel) recorded over Nairobi on day of year (DOY) 171 (a) and 267 (b) in 2011. The red curves in the top panels are the median drift velocity values over a running window of 5 min.

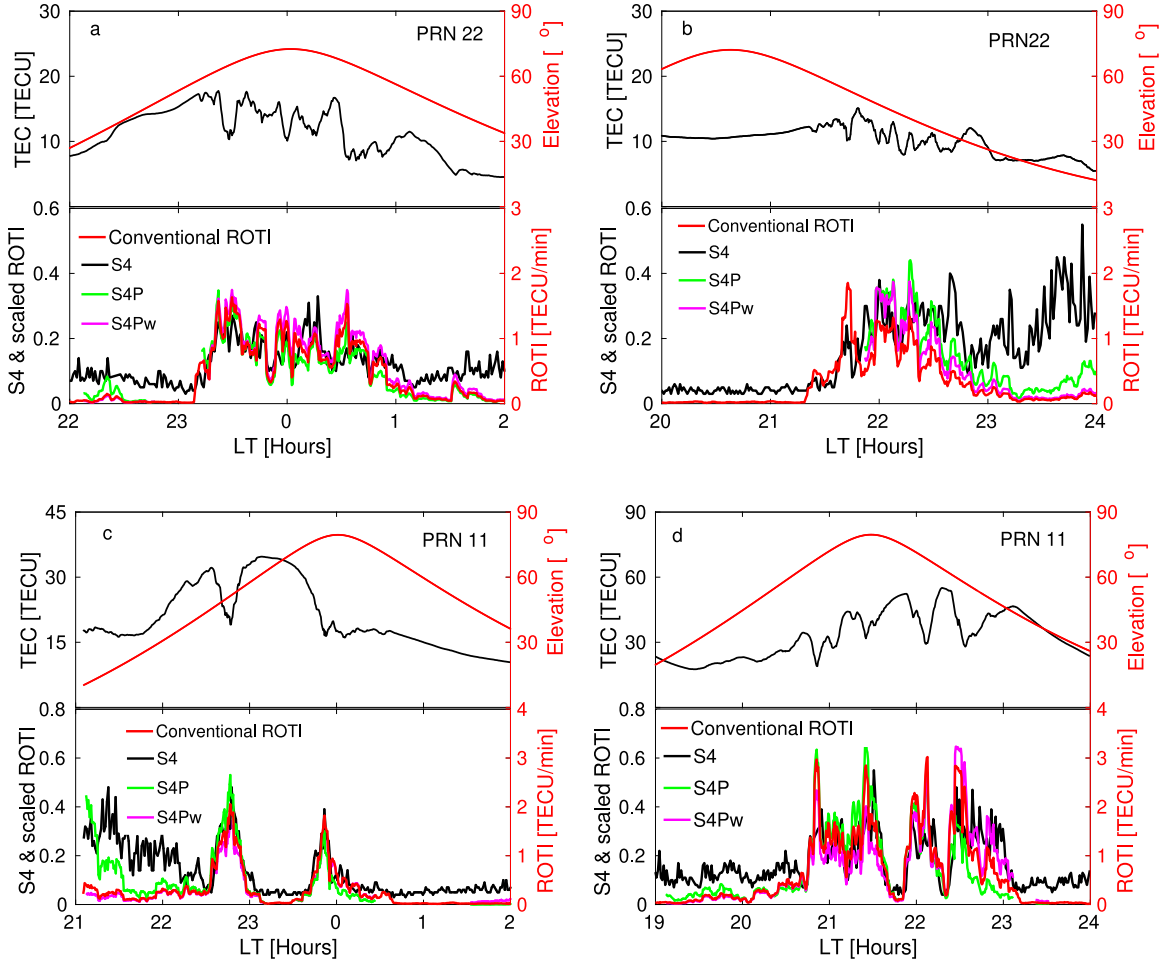


Fig. 2. Variation of TEC, ROTI and S4 over Nairobi on DOY 165 (a), 215 (b), 263 (c) and 300 (d) in 2011.

encountered density irregularities between 21:20 and 23:00 LT on DOY 215 in 2011. Moderate scintillation with S4 reaching ~0.3 were recorded by the SCINDA at Nairobi. The conventional ROTI reached a value of 1.4 TECU/min at the time when the signal encountered the density irregularities. Similarly both S4P and S4Pw produced a better qualitative estimate of S4 than the conventional ROTI. However, at lower elevation angles, both S4P and S4Pw underestimated the S4. Another case of scintillation occurring at high elevation angle are shown in Fig. 2 c and d. The scintillation on DOY 263 is possibly due to two different clouds of irregularities that intercepted radio signals from PRN 11 between 22:30

and 22:00 LT, and between 23:40 and 24:00 LT. While on DOY 300, a number of scintillation patches were observed probably due to a number of density irregularities that intercepted the signals from PRN 11 between 20:50 and 23:00 LT. In both of these cases, though some differences were observed between S4P and S4Pw, they each numerically matched S4 from the co-located SCINDA better than the conventional ROTI.

Though both S4P and S4Pw produced better matches with S4, we further investigated which of these methods produced better correlation with the S4 values. In the correlation analysis, the 30 s sampled data were first down sampled to 5 min (interval over which ROTI is often computed) by averaging all data values corresponding to all the satellites in view at elevations greater than 40°. The choice of the higher elevation angle was because a better correlation between S4 and scaled ROTI was observed at higher elevation angles. The S4 observations at elevations greater than 40° were also averaged over 5 min to match the sampling rate of the ROTI. We then determined the Pearson linear correlation coefficient r, between the 5 min data samples. Fig. 3 and Table 2 show the results of the correlation analysis for some days when the drift velocity data was available.

From Table 2 and Fig. 3, both S4P and S4Pw show a strong positive correlation (r ≈0.6071–0.9293) with S4. Notable in Fig. 3 is the positive bias of ~0.05 between S4 and the scaled ROTI. This bias could be due to the noise term in the S4 which unlike in the scaled ROTI does not average to nearly zero but rather to a value of ~0.05.

A Comparison of the correlation coefficients for S4P and S4Pw show that for the majority of the scintillation events studied, S4P was better correlated with S4 than S4Pw. This difference could be due to the unknown spectral index ν which was assumed to be constant in this work. However, the differences in the correlation coefficients for the individual scintillation events is not significant. Therefore any of the two approaches could be used to scale ROTI in order to estimate S4 if the zonal drift velocity of irregularities and the spectral index (for the case of method2) can be reliably estimated. This observation suggests that the scaling factors γ and α are approximately the same. However, due to absence of high rate data from which the spectral index ν is often estimated, we adopted equation 4 to obtain the S4 proxy which we used to further study scintillation climatology over Nairobi. First, the available ion drift velocity data from the VHF receiver at Nairobi was used to study and model the zonal irregularity drift velocities. We expressed the irregularity drift velocities as a function of time (t), month (m) and solar radio flux measured at 10.7 cm wavelength (F10.7), a proxy of extreme ultraviolet radiation as

Table 2
Correlation analysis for other scintillation events studied.

	Corr. coefficient with S4			Corr. coefficient with S4	
Event date	S4P	S4Pw	Event date	S4P	S4Pw
2011-03-31	0.8744	0.7812	2011-08-03	0.8331	0.8452
2011-04-10	0.6411	0.7235	2011-08-07	0.6773	0.6847
2011-04-14	0.8249	0.6866	2011-09-22	0.8394	0.7311
2011-04-18	0.6407	0.6071	2011-09-24	0.8546	0.8400
2011-04-22	0.7871	0.7561	2011-10-25	0.8678	0.8646
2011-04-28	0.8315	0.8342	2011-10-27	0.7993	0.6903

$$V_{(t,m,F10.7)} = a_o + a_1 t + a_2 \cos\left(\frac{\pi t}{12}\right) + a_3 \sin\left(\frac{\pi t}{12}\right) + a_4 \cos\left(\frac{\pi m}{6}\right) + a_5 \sin\left(\frac{\pi m}{6}\right). \quad (11)$$

The coefficients a_o to a_5 in equation (11) were determined by least square fit to the VHF data. Fig. 4 shows the local time variation of the monthly averaged 5 min zonal irregularity drift velocities and their predicted values from equation (11) for the month of June (Fig. 4 a) and September (Fig. 4 b).

Fig. 4 shows that the irregularities had a higher velocity in September than in June. Such differences were replicated for all the months. These differences could be due to the variation of the thermospheric neutral winds driven by the temperature variations in the different months. The predicted zonal drift velocities give a good estimate of the observed monthly averaged irregularity drift velocities. Well aware of the limited VHF data used to constrain the coefficients in equation (11), we adopted equation (11) to estimate the zonal drift velocity of the irregularities in scaling ROTI for days with no VHF data. This approach is different from that of Amabayo et al. (2015) where they used a constant velocity of 120 m/s as an estimate for the zonal drift velocity of the irregularities. The scaled ROTI was used as a proxy for S4 which we then used in our further analysis of scintillation activity over Nairobi.

3.3. Temporal variation of scintillation

In this subsection, the aim is to compare the scintillation climatology using data from co-located IGS and SCINDA receivers. The S4 and S4P were obtained for all the available data from the Nairobi SCINDA and IGS receivers. Fig. 5 shows the scintillation climatology maps over Nairobi in 2011 derived from the SCINDA (a) and the IGS (b) data.

To generate the maps, the daily 5 min averages of S4 and S4P for all

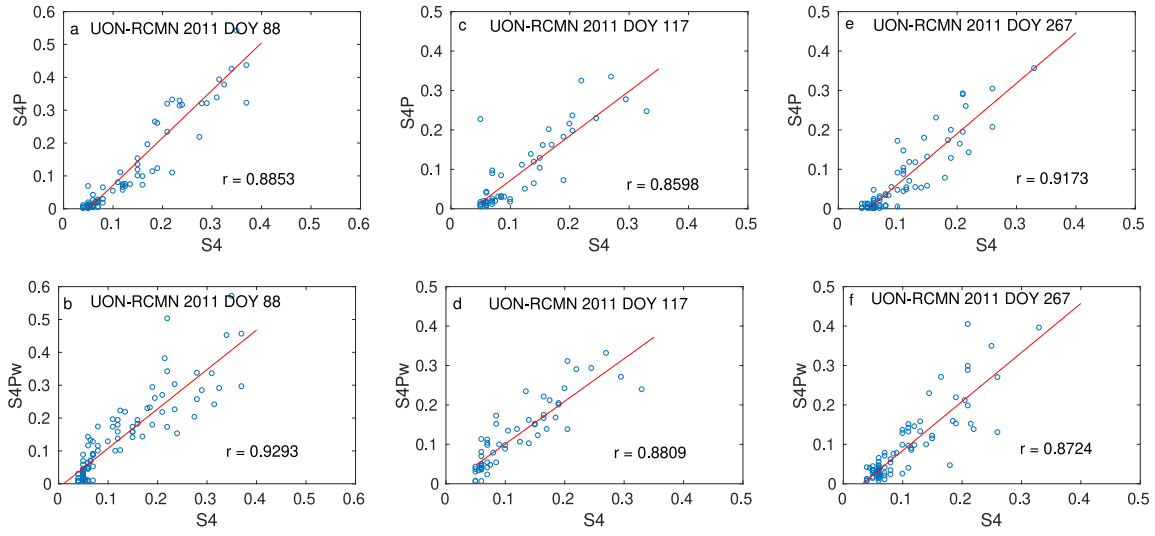


Fig. 3. Correlation analysis between scaled ROTI and S4.

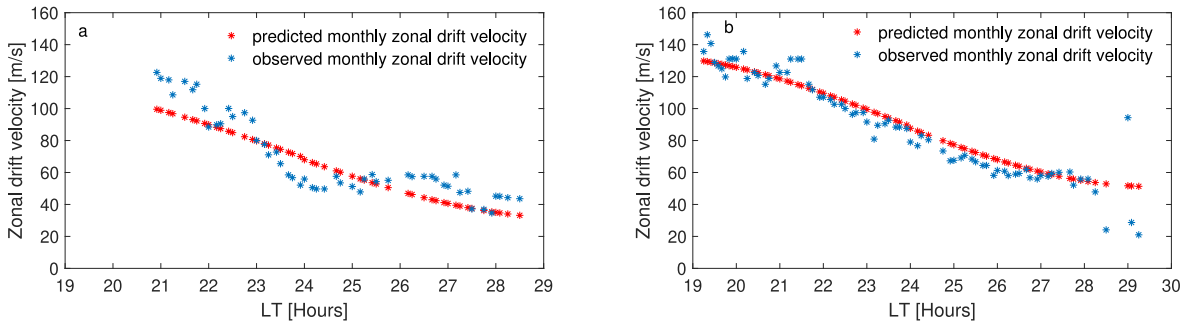


Fig. 4. Local time variation of zonal drift velocities of equatorial irregularities obtained from spaced receiver measurements at Nairobi (blue curve) and their predicted values (red curve) for June and September in 2011.

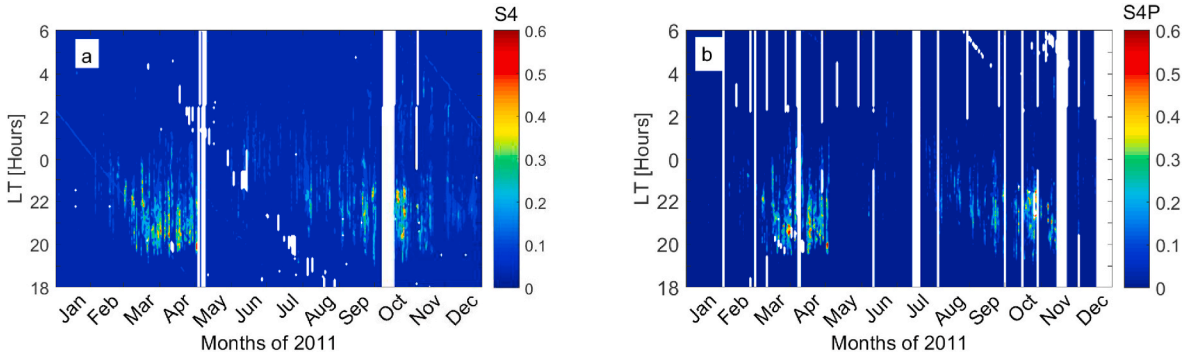


Fig. 5. Contour maps of S4 (a) and S4P (b) over Nairobi in 2011.

visible satellites at elevations greater than 40° were used. The scintillation climatology obtained using S4 (Fig. 4 a) and S4P (Fig. 4 b) are similar. The highest values of S4 and the S4P were observed in the equinox months of March–April and September–October. The local time variation of scintillation occurrence was in conformity with the already known nocturnal behavior of the equatorial scintillation. The local time peak was observed between 21:00 and 23:00 LT. These observations further emphasize that, when appropriately scaled, ROTI may be used to characterize scintillation in the same way as with S4. Fig. 6 illustrates the use of S4P for filling data gaps in SCINDA data for a typical case when scintillation and TEC data over Mbarara covered different periods in 2015.

Fig. 6 a shows that there was no scintillation data before April. While in Fig. 6 c the gap in the scintillation data has been filled with S4P shown in Fig. 6 b. The excellent match further confirms the usefulness of our method of scaling ROTI. Unlike in most approaches of scaling ROTI where the scaling factor between S4 and ROTI is derived from correlation analysis, our scaling is based on the theoretical formulation. This approach is similar but less complex to the one used in Carrano et al. (2019) to scale ROTI to match S4 which requires the irregularity spectral index that is often obtained from high rate data. The scaled ROTI will therefore help to improve on low latitude scintillation climatology since there are more IGS receivers than scintillation monitors deployed over the low latitude region.

3.4. Model results

The solar activity dependence of the occurrence probability of ionospheric scintillation over Nairobi is presented for three solar flux bins of F10.7<80 (Fig. 7 a & b), 80≤F10.7<120 (Fig. 7 c & d) and F10.7≥120 (Fig. 7 e & f).

Fig. 7 a, c and e show the probabilities derived from the combined data sets of S4 and S4P while Fig. 7 b, d and f are their model predicted values. The model very well predicted the observed monthly and local time occurrence probabilities of scintillation over Nairobi. This suggests that the monthly and the local time nodes used in modeling the scintillation occurrence appear to be sufficient. Fig. 7 shows that there is a higher likelihood of scintillation occurrence during high solar activity periods than during medium and low solar activity periods. The chances of scintillation occurring during low solar activity were very small. The local time scintillation occurrence peaked between 20:00–23:00 LT in all the solar activity bins. The seasonal occurrence of scintillation over

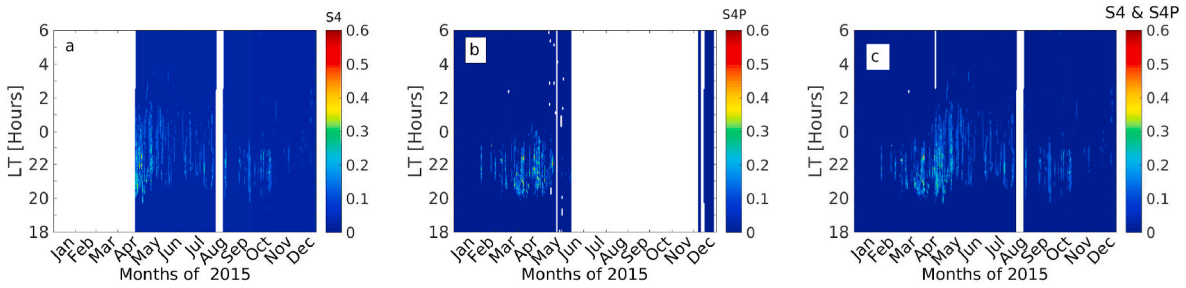


Fig. 6. Contour maps of S4 (a), S4P (b) and S4 combined with S4P (c) over Mbarara in 2015.

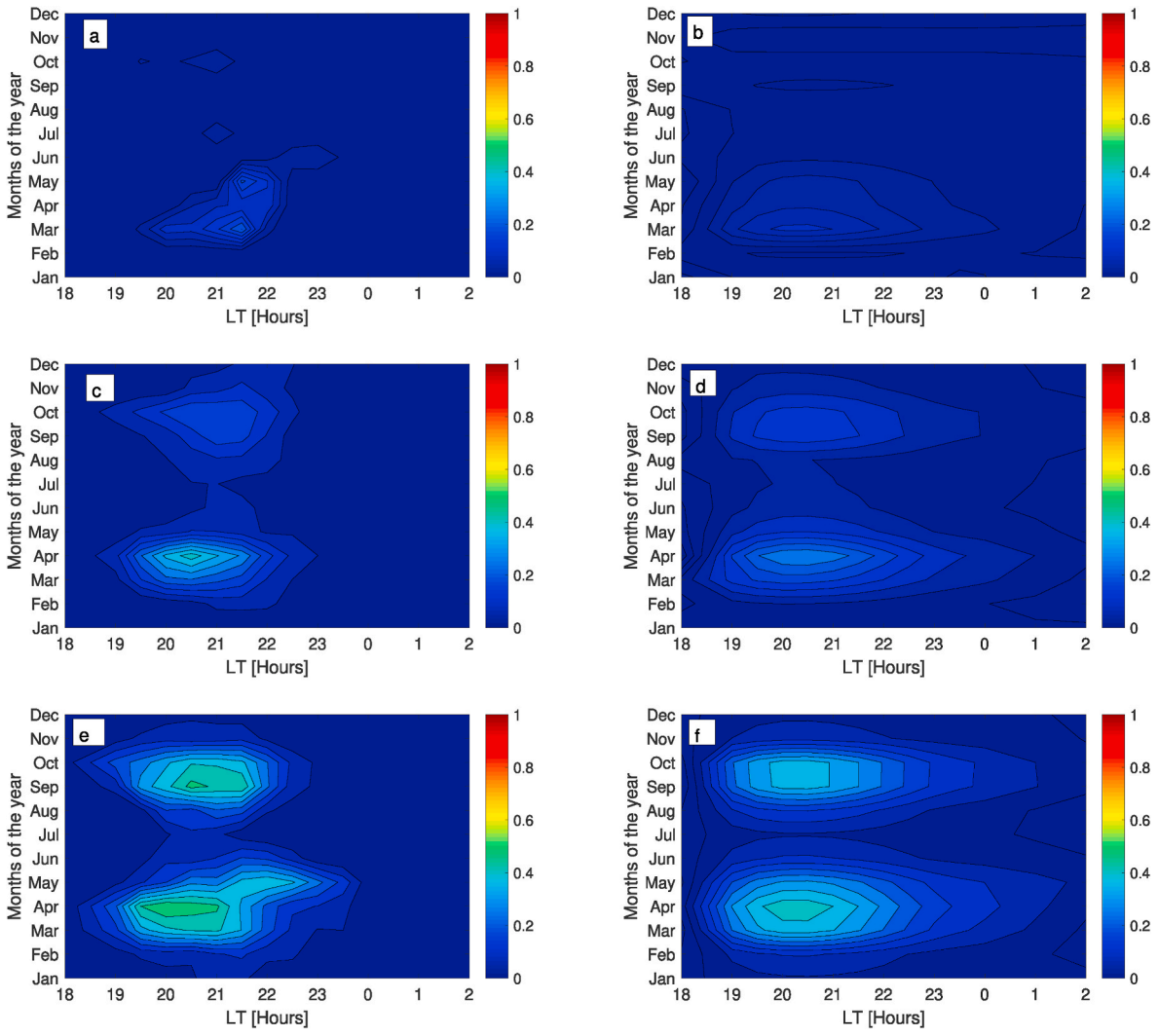


Fig. 7. Scintillation occurrence probabilities over Nairobi derived from S4 combined with S4P (a, c and e) and the model predicted values (b, d and f) for solar flux ranges of F10.7<80 (a nd b), 80≤F10.7<120 (c and d) and F10.7≥120 (e and f). The color bar represents the probability of occurrence of scintillation.

Nairobi is more frequent during the equinox months than during the solstices. The scintillation climatology also revealed a clear equinoctial asymmetry with scintillation occurrence over Nairobi being less frequent during vernal equinox than the autumnal equinox. This observation is consistent with the results of similar studies (e.g Olwendo et al., 2013; Mungufeni et al., 2016) over the East African region. Equinoctial asymmetry in the occurrence of ionospheric irregularities and hence scintillation has also been reported in literature for other longitude sectors (e.g. Otsuka et al., 2006; Nishioka et al., 2008; Sripathi et al., 2011). Otsuka et al. (2006) reported higher occurrence of scintillation and higher zonal drift velocity of irregularities during the March–April equinox than the September–October equinox in Indonesia. They attributed the differences in the occurrence of scintillation during the March–April equinox and the September–October equinox to the asymmetry in the zonal drift velocity of irregularities. Following Otsuka et al. (2006), the asymmetry in the occurrence of scintillation over Nairobi observed in this study could be due to the higher zonal drift velocity of irregularities during the autumnal equinox than during the vernal equinox (Olwendo et al., 2013). Andima et al. (2018) observed that the nighttime zonal drift velocity of ions is in the same range as the zonal drift velocity of irregularities. This implies that the zonal drift velocity of the ions over Nairobi is higher during the autumnal equinox than during the vernal equinox. Since the zonal drift velocity of the ions is approximately the same as the zonal component of the neutral gas velocity (Heelis, 2004), the ion drift velocities may be used as a proxy for the neutral wind velocity. This therefore suggests that the velocity of neutral wind over Nairobi is higher during the autumnal equinox than during the vernal equinox. The post sunset eastward neutral wind creates $U \times B$ vertical polarization electric field through the F dynamo mechanism. The vertical polarization electric field drives an eastward zonal electric field that enhances the already eastward post sunset ambient electric field. The higher neutral wind velocity during the autumnal equinox than during the vernal equinox results in a higher eastward electric field associated with the neutral wind during the autumnal equinox than during the vernal equinox. The effect of increased eastward electric field is the rapid lifting of the F-region to higher altitudes, thus creating favorable conditions for development of the Rayleigh Taylor instability that is known to be responsible for the generation of equatorial irregularities. These irregularities cause scintillation when radio signals pass through them. This could explain the higher likelihood of occurrence of scintillation during the autumnal equinox than the vernal equinox. However, the cause for the equinoctial asymmetry in the neutral wind velocity over Nairobi requires further investigation.

3.5. *Application of the model and future work*

The findings of this work can be used for predicting the likelihood of

occurrence of amplitude scintillation over Nairobi. Incorporated in the scintillation proxy model is a velocity model which can be used to study the climatology of the zonal drift velocity of irregularities over Nairobi. We are currently working on extending the velocity model to other parts of Africa with a view of producing a regional spatial zonal drift velocity model. This is to be achieved by incorporating zonal ion drift velocities measured by low earth orbiting satellites since some earlier studies (e.g. Andima et al., 2018) have shown that the zonal ion drift velocities derived from the satellite data are comparable to the zonal drift velocity of the irregularities measured by the spaced receiver technique. The spatial velocity model is a key step towards extending the scintillation proxy model to a regional model over the African low latitudes. Such a regional model will facilitate the generation of scintillation maps from the ever increasing number of GNSS data sources in the African low latitudes.

4. Conclusion

We have scaled ROTI to match S4 derived from a SCINDA receiver over a low latitude region. Such a scaling has been presented and validated before (e.g. Du et al., 2000; Amabayo et al., 2015). Besides the work presented in these earlier papers, we have incorporated the fact that the velocity of the ray path and that of the irregularities are not constants. The irregularity drift velocities were derived from the spaced receiver measurements. A very good match was obtained between the scaled ROTI and S4 from co-located receivers. For the first time, the scaled ROTI was combined with S4 to model the likelihood of scintillation occurrence. The model results were in good agreement with the observations. The likelihood of occurrence of scintillation was higher during the autumnal equinox than during the vernal equinox for all the solar activity levels. This suggests that in a theoretical scintillation model over the low latitude region of East Africa, the behaviors of the plasma density irregularities during the March–April equinox should be distinguished from that during the September–October equinox. The local time occurrence probability of scintillation peaked between 20:00 LT and 23:00 LT. Due to the relatively large data set used in this analysis, we are confident that the results in this analysis give a representation of scintillation climatology over Nairobi for the different solar activity periods.

Declaration of competing interest

The authors declare that they have no known competing financial interests or personal relationships that could have appeared to influence the work reported in this paper.

Acknowledgement

Financial support from International Science Programme (ISP) of Uppsala University in Sweden. We acknowledge the administration and staff of the Space Science Directorate of the South African National Space Agency (SANSA) for the support during the research visit of the first author to the institution. The ionospheric scintillation and total electron content monitors of the SCINDA network, from which the scintillation data used in this study were obtained, were supplied by the Air Force Research Laboratory in coordination with Boston College, USA. The IGS data used in this study was obtained from ftp://cddis.gsfc.nasa.gov/. The precise orbit files which we used to calculate the ray path velocities were obtained from ftp://ftp.nga.mil/pub2/gps/apcpe/.

References

Aarons, J., Mendillo, M., Yantosca, R., 1997. GPS phase fluctuations in the equatorial region during sunspot minimum. Radio Sci. 32, 1535–1550.
Aarons, J., Mendillo, M., Yantosca, R., Kudeki, E., 1996. GPS phase fluctuations in the equatorial region during the MISETA 1994 campaign. J. Geophys. Res. 101, 26851–26862.
Abdu, M.A., Souza, J.R., Batista, I.S., Sobral, J.H.A., 2003. Equatorial spread F statistics and empirical representation for IRI: a regional model for the brazilian longitude sector. Adv. Space Res. 31, 703–716.
Amabayo, E.B., Jurua, E., Cilliers, P.J., 2015. Validating the use of scintillation proxies to study ionospheric scintillation over the Ugandan region. J. Atmos. Sol. Terr. Phys. 128, 84–91.
Andima, G., Amabayo, E.B., Jurua, E., Cilliers, P.J., 2018. Characterization of the low latitude plasma density irregularities observed using C/NOFS and SCINDA data. Adv. Space Res. 61, 264–273.
Basu, S., Groves, K.M., Quinn, J.M., Doherty, P., 1999. A comparison of TEC fluctuations and scintillations at Ascension Island. J. Atmos. Sol. Terr. Phys. 61, 1219–1226.
Beach, T.L., Kintner, P.M., 2009. Simultaneous Global Positioning System observations of equatorial scintillations and total electron content fluctuations. J. Geophys. Res. 104, 22553–22565.
Bhattacharya, S., Purohit, P.K., Gwal, A.K., 2009. Ionospheric time delay variations in the equatorial anomaly region during low solar activity using GPS. Indian J. Radio Space Phys. 38, 266–274.
Carrano, C.S., Groves, K.M., 2010. Temporal decorrelation of GPS satellite signals due to multiple scattering from ionospheric irregularities. Proceedings of the 23rd International Technical Meeting of the Satellite. Division of the Institute of Navigation, pp. 361–374 (ION GNSS 2010).
Carrano, C.S., Groves, K.M., Rino, C.L., 2019. On the relationship between the rate of change of total electron content index (ROTI), irregularity strength (CkL) and the scintillation index (S4). J. Geophys. Res. Space Phys. 124 https://doi.org/10.1029/2018JA026353.
Carrano, C.S., Groves, K.M., Rino, C.L., Doherty, P.H., 2016. A technique for inferring zonal irregularity drift from single station GNSS measurements of intensity (S) and phase (σ_ϕ) scintillations. Radio Sci. 51 https://doi.org/10.1002/2015RS005864, 4.
Du, J., Wilkinson, P., Thomas, R., Cervera, M., 2000. Determination of equatorial ionospheric scintillation S4 dual frequency GPS. URSI Commission G, Workshop. La Trobe University, Australia.
Heelis, R., 2004. Electrodynamics in the low and middle latitude ionosphere: a tutorial. J. Atmos. Terr. Phys. 66, 825–838.
Iyer, K.N., Souza, J.R., Pathan, B.M., Abdu, M.A., Jivani, M.N., Joshi, H.P., 2006. A model of equatorial and low latitude VHF scintillation in India. Indian J. Radio Space Phys. 35, 98–104.
Kelley, M.C., 2009. The Earth's Ionosphere: Plasma Physics and Electrodynamics, second ed. Amsterdam academic Press.
Mungufeni, P., Habarulema, J.B., Jurua, E., 2016. Trends of ionospheric irregularities over African low latitude region during quiet geomagnetic conditions. J. Atmos. Sol. Terr. Phys. 138 (139), 261–267.
Mungufeni, P., Jurua, E., Habarulema, J.B., Katrini, S.A., 2015. Modelling the probability of ionospheric irregularity occurrence over African low latitude region. J. Atmos. Sol. Terr. Phys. 128, 46–57.
Nishioka, M., Saito, Tsugawa, T., 2008. Occurrence characteristics of plasma bubble derived from global ground-based GPS receiver networks. J. Geophys. Res. 113, A05301.
Olwendo, O., Baluku, T., Baki, P., Cilliers, P., Mito, C., Doherty, P., 2013. Low latitude ionospheric scintillation and zonal irregularity drifts observed with GPS-SCINDA system and closely spaced VHF receivers in Kenya. Adv. Space Res. 51, 1715–1726.
Otsuka, Y., Shiokawa, K., Ogawa, T., 2006. Equatorial ionospheric scintillations and zonal irregularity drifts observed with closely-spaced GPS receivers in Indonesia. J. Met. Soc. Japan 84A, 343–351.
Pi, X., Mannucci, A.J., Lindqwister, U.J., Ho, C.M., 1997. Monitoring of global ionospheric irregularities using the worldwide GPS network. Geophys. Res. Lett. 24, 2283–2286.
Rao, P.V.S.R., Ram, S.T., Niranjan, K., Prasad, D.S.V.V.D., Krishna, S.G., Lakshmi, N.K. M., 2005. VHF and L-band scintillation characteristics over Indian low latitude station, Waltair (17.7 N, 83.3E). Ann. Geophys. 23, 2457–2464. ∘-∘.
Rino, C.L., 1979. A power law phase screen model for ionospheric scintillation: 1. weak scatter. Radio Sci. 14, 1135–1145.
Seemala, G.K., Valladares, C.E., 2011. Statistics of total electron content depletions observed over the South American continent for the year 2008. Radio Sci. 46, RS5019.
Sripathi, S., Kakad, B., Bhattacharyya, A., 2011. Study of equinoctial asymmetry in the Equatorial Spread F (ESF) irregularities over Indian region using multi-instrument observations in the descending phase of solar cycle 23. J. Geophys. Res. 116, A11302.
Teague, M.R., 1983. Deterministic phase retrieval: a Green's function solution. J. Opt. Soc. Am. 73, 1434–1441.
Zou, Y., Wang, D., 2009. A study of GPS ionospheric scintillations observed at Guilin. J. Atmos. Terr. Phys. 71, 1948–1958.